2024 IEEE International Conference on Robotics and Automation (ICRA 2024)
May 13-17, 2024. Yokohama, Japan

Simulation and Experimental Validation of an Autonomous Perching and Takeoff Method for a Multirotor UAV on Vertical Surfaces using a Suction Cup

Bruno Chapdelaine[1], Mathis Celce[2], Charles Vidal[1], Lionel Birglen[3], Bruno Monsarrat[1]

***Abstract*— This paper details the simulation and experimental validation of an autonomous perching and take-off method for a multirotor unmanned aerial vehicle (UAV) using a suction cup perching mechanism on vertical surfaces. The suction cup interaction with different surface types is characterized with experimental tests to accurately model the perching manoeuvre. The resulting model is used to develop a realistic hardware-in-the-loop (HIL) simulation of the perching and take-off manoeuvre of the UAV in Gazebo. A control method is developed to automate the perching and take-off manoeuvre. The method is tested in simulation and is experimentally validated with flight tests. Comparisons between simulation and experimental data demonstrate that the simulation is accurate and can be used to continue the development of autonomous perching methods.**

I. Introduction

The use of Unmanned Aerial Vehicles (UAVs) for inspection and maintenance has seen a great increase in the past decade. Their manoeuvrability and ease of deployment allows them to efficiently reach structures that would be dangerous and time consuming for a technician to access. UAVs are used to inspect buildings [1], dams [2], power lines [3] and wind turbine blades [4]. Unfortunately, their limited flight time is a major constraint for contact tasks and surveillance applications. To extend their operational time, UAVs can interact with structures by leaning or perching on them as shown in [5]. Turning off the motors when perched significantly reduces the energy consumption of the UAV but interacting with a structure is a complex flight operation.

Manual perching manoeuvres require a highly skilled pilot and pose a greater risk of crashing the aircraft. The complexity of the manoeuvre is also highly dependant on external parameters such as visibility from the ground, weather, clearance around the target, wind interaction with the structure, etc. Automating perching manoeuvres is an attractive solution to ensure safe, robust and repeatable perching.

Perching UAVs using suction cups have been presented by [6], [7] and [8]. These developments relied on experimental tests to develop the perching mechanisms. An autonomous perching procedure for a UAV with a suction cup was presented in [9] where the control strategy was developed with experimental flight tests. Due to the inherent risk of crashing aerial vehicles, developing a control strategy with flight tests can be a costly and time consuming approach.

Many open-source simulators can be used to develop autonomous solutions for UAVs like Gazebo [10], Airsim [11], OpenUAV [12] and XTDrone [13]. However, these simulators mostly focus on flight and sensor simulation for the development of guidance, navigation, and control capabilities. Perching is a niche UAV application and custom plugins need to be developed in order to test perching mechanisms in a simulator.

In this research, a perching UAV using a suction cup is presented and modeled in Gazebo. The suction cup is characterized with experimental tests and a custom perching plugin for Gazebo is developed. The simulation is used to develop an autonomous perching method with hardware-in-the-loop (HIL). It is validated with flight tests and the experimental data is compared with the simulation.

The paper is organized as follows. The UAV design and model are presented in Section II followed by the customization of the simulation environment in Section III. An autonomous perching method is presented in Section IV and finally a comparison between the experimental tests and the simulation is presented in Section V.

II. UAV Design and Model

A. Dynamic Model

The inertial frame $\mathcal{W} = \{\mathbf{w}_1, \mathbf{w}_2, \mathbf{w}_3\}$ is of type north-east-down (NED). The UAV body-fixed frame is defined by $\mathcal{B} = \{\mathbf{b}_1, \mathbf{b}_2, \mathbf{b}_3\}$ and its origin is located at the centre of mass of the UAV. The orientation of the body frame relative to the inertial frame is defined by three rotations : roll ϕ, pitch θ and yaw ψ. The equations of motion of the UAV are given by:

$$m\ddot{\mathbf{x}} = \mathbf{R}_B^W \mathbf{F} \tag{1}$$

$$\mathbf{I}\dot{\boldsymbol{\omega}} + \boldsymbol{\omega} \times (\mathbf{I}\boldsymbol{\omega}) = \mathbf{M} \tag{2}$$

where:

- $\mathbf{x}$ the position of the body frame in the inertial frame,
- $\boldsymbol{\omega}$ the angular velocity of the body frame,
- $\mathbf{R}_B^W$ the rotation matrix from the body frame to the inertial frame

*This work was supported by the NRC's Integrated Aerial Mobility (IAM) program.

[1]B. Chapdelaine, C. Vidal and B. Monsarrat are with the NRC's Aerospace Research Centre, Montréal, QC, CAN, bruno.chapdelaine@cnrc-nrc.gc.ca

[2]M. Celce is a MSc. student at Polytechnique Montréal, Montréal, QC, CAN, mathis.celce@polymtl.ca

[2]L. Birglen is a professor at Polytechnique Montréal, Montréal, QC, CAN, lionel.birglen@polymtl.ca

- **F** and **M** the total force and moment vectors acting on the body frame,
- **I** and m the inertia matrix and the mass of the UAV

B. UAV Design

The UAV is a custom-built quadrotor with a diagonal wheelbase of 58 cm and a total mass of 3.2 kg including the companion computer, the additional sensors and the perching mechanism. It uses 3508 380KV brushless motors with 1255 carbon fiber propellers and a 6S 4000 mAh battery.

The perching mechanism is shown in Fig. 1. It is composed of a 3D printed epoxy coated suction cup with a spring sliding mechanism, two carbon fiber tubes fixed to the UAV and two carbon fiber legs. The legs limit the pitch when perched. The purpose of the slider is to extend the contact duration between the suction cup and the surface at the time of impact. The vacuum pump is located at the back of the UAV to balance the aircraft. The joint between the cup and the sliding mechanism has two degrees of freedom.

The suction cup is equipped with a pressure sensor and the perching mechanism has a force sensor integrated. The UAV is equipped with two Benewake TFmini Plus single-point LiDARs, one on each front arm pointing forwards parallel to $\mathbf{b_1}$.

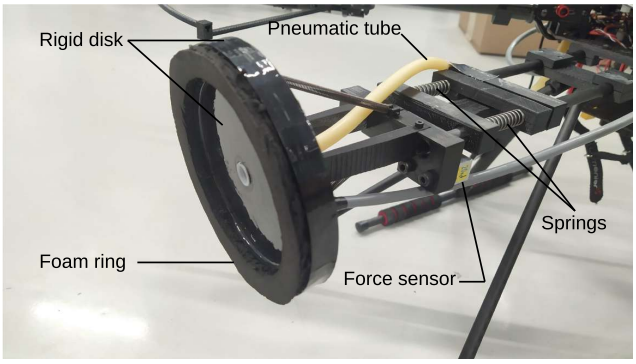

Fig. 1. Perching device used for the experiments.

To create the UAV model in Gazebo, the aircraft is modeled in Solidworks with the perching mechanism. The CAD model is converted into a URDF file (Universal Robot Description Format) using the SW2URDF plugin in SolidWorks. The URDF is imported in Gazebo and converted into a SDF that keeps the visuals, links and joints of the CAD model.

C. Rotor model

The gazebo motor and propeller model is used to model the powertrain of the UAV. It is a simple propeller model that has been modified to better model multirotors. It uses a non-standard notation and it is further explained in [14]. The motor constant k_{mot} and the moment constant k_{mom} are defined as :

$$k_{mot} = \frac{C_{T0}\rho D^4}{4\pi^2} \tag{3}$$

$$k_{mom} = \frac{C_{Q0}}{C_{T0}} D \tag{4}$$

where:

- C_{T0} and C_{Q0} are the static thrust and torque coefficients,
- D is the propeller diameter,
- and ρ is the air density.

Parameters C_{T0} and C_{Q0} can be found using the UIUC airfoil database[1]. The parameters used in the simulation are shown in Table I.

TABLE I
GAZEBO MOTOR MODEL PARAMETERS

	Iris UAV (default parameters)	Perching UAV
k_{mot} (kg ∗ m)	5.84×10^{-6}	2.5×10^{-5}
k_{mom} (m)	6.00×10^{-2}	1.9×10^{-2}
λ_1 (kg)	1.75×10^{-4}	8×10^{-4}

D. Suction cup model

To model the behavior of the suction cup during perching, the pressure inside the cup has been measured as a function of time when pressed on different surface types. The pressure can be approximated by the following equations:

$$\text{Sealing}: P(t) = \mathrm{P_{vac}} + (\mathrm{P_{atm}} - \mathrm{P_{vac}})e^{-t/\tau_1} \tag{5}$$

$$\text{Unsealing}: P(t) = \mathrm{P_{atm}} - (\mathrm{P_{atm}} - \mathrm{P_{vac}})e^{-t/\tau_2} \tag{6}$$

where $P(t)$ is the instantaneous pressure in the suction cup. P_{vac} is the minimal pressure achievable in steady state, P_{atm} is the atmospheric pressure and τ_i $(i = 1, 2)$ are the time constants. The equation parameters are listed in Table II. Fig. 2 shows the sealing pressure profiles in dashed lines and the measurements by surface type. The decrease of pressure in the suction cup is the slowest on a porous concrete wall compared to a painted cinder block and a wind turbine blade. Similarly, the vacuum level reached on concrete is the lowest of all the surfaces tested because of the higher porosity of the material and the greater surface roughness.

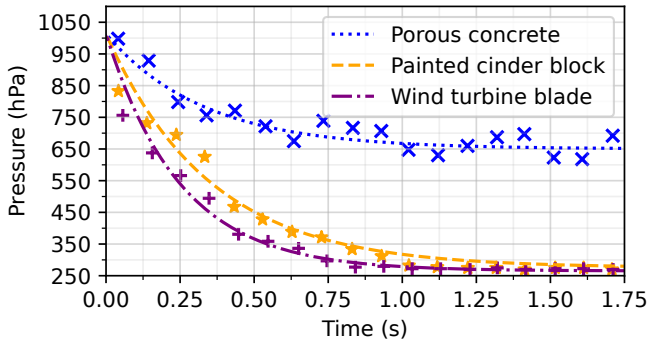

Fig. 2. Measured pressure inside the suction cup when pressed on various surfaces as a function of time.

On rough and porous surfaces, the suction cup needs to be pressed with enough force against the surface to create a

[1]https://m-selig.ae.illinois.edu/

TABLE II

SUCTION CUP PRESSURE MODEL PARAMETERS FROM EXPERIMENTS ON VARIOUS SURFACES.

	Porous concrete	Cinder block	Wind turbine blade	Metallic surface
P_{vac} (hPa)	650	275	265	275
τ_1 (s)	0.33 ± 0.03	0.35 ± 0.03	0.25 ± 0.03	0.25 ± 0.03
τ_2 (s)	0.40 ± 0.03	7.5 ± 0.5	8.0 ± 0.5	16 ± 1

tight seal until the vacuum inside the cup is strong enough for it to stay engaged. To accomplish that, the UAV needs to hit the surface with moderate velocity perpendicular to it. Fig. 3 shows the probability of a successful perching on a vertical porous concrete wall as a function of the impact speed obtained from 253 experiments conducted with the UAV and a 5 m long pendulum. A perching attempt is considered successful when the suction cup attaches to the surface.

According to Fig. 3, the best results are obtained at an impact speed between 1 and 1.2 m.s^{-1}. At speeds below 0.4 m.s^{-1}, the impact does not apply enough force on the suction cup. At speeds over 1.2 m.s^{-1}, the manoeuvre is deemed too dangerous for the UAV. Some of the randomness in the success rate can be attributed to the variable surface roughness of the concrete surface and slight misalignment between the suction cup and the surface on impact.

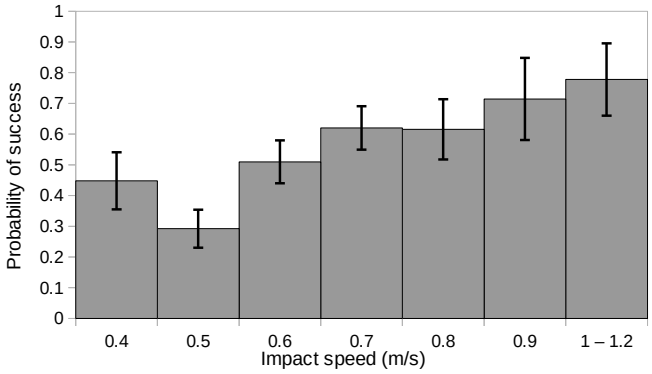

Fig. 3. Probability of a successful attachment of the perching device relative to the impact speed.

E. Control Architecture

The UAV is controlled by a Pixhawk autopilot with the PX4 flight stack and a Raspberry Pi companion computer running Ubuntu 20.04. It is flown in offboard control mode and controlled from a ROS script. An OptiTrack motion capture system is used to simulate a GPS signal indoors. The motion capture software Motive is running on the ground control station and streams the position and orientation of the UAV to the Raspberry Pi companion computer via WiFi. The motion capture data is then remapped and fed to the Extended Kalman Filter (EKF) state estimator of the autopilot.

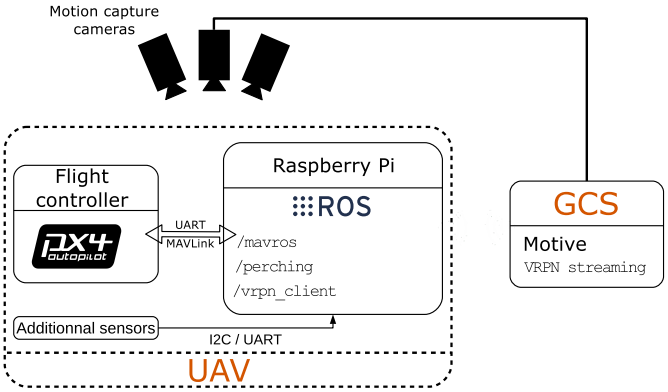

Fig. 4. Control architecture of the UAV showing the interaction between the companion computer, the autopilot and the Ground Control Station (GCS).

III. CUSTOMIZATION OF THE SIMULATION ENVIRONMENT

A. Software Architecture

The simulation environment is developed in the open-source Gazebo 11 robotics simulator on Ubuntu 20.04 using ROS and PX4 HIL. Fig. 5 shows the software architecture of the simulation environment. Gazebo handles the dynamic simulation of the aircraft, the sensors and the physical interactions between the UAV and the environment. ROS packages handle the perching automation and the perching plugin.

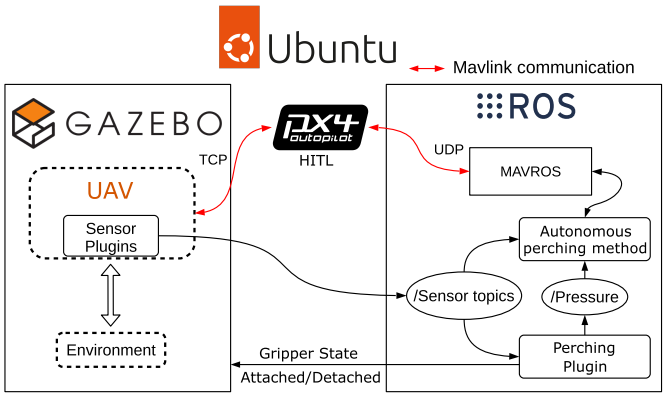

Fig. 5. Software architecture of the simulation environment.

B. Perching Mechanism Plugin

To simulate the perching mechanism, a ROS package and a Gazebo plugin are developed. The ROS package contains nodes that run the suction cup model and the logic control of the Gazebo plugin. The plugin is based on the Gazebo ROS link attacher plugin and it allows the creation of a joint between two links. It is called under certain conditions to attach or detach the suction cup on the surface.

A joint is created when the impact force is above the sealing threshold and the suction cup has been in direct contact with the surface for the time required for the pressure

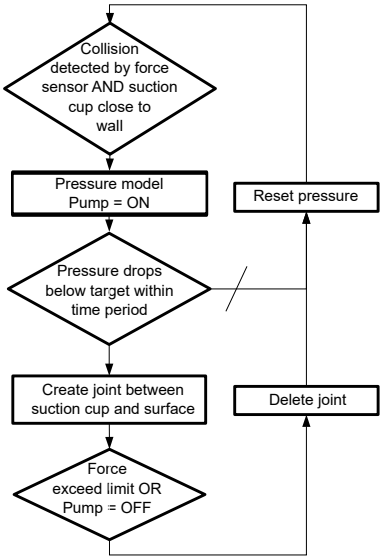

Fig. 6. Overview of the perching mechanism plugin algorithm.

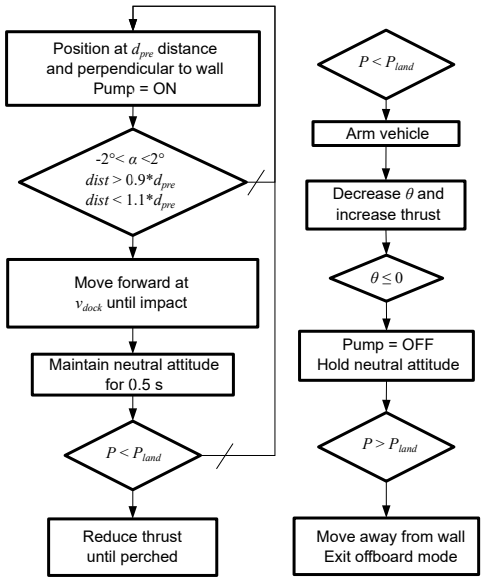

Fig. 7. Overview of the autonomous perching method. Preliminary positioning and perching sequence (left), takeoff and detachment sequence (right).

to drop below the attachment threshold. An overview of the perching plugin algorithm is shown in Fig. 6.

IV. Autonomous Perching Sequence

The perching sequence uses the two front facing LiDARs to measure the angle α between the vertical surface and the UAV and the distance between the UAV and the surface. The angle α is given by :

$$\alpha = \arctan \frac{d_1 - d_2}{l} \tag{7}$$

where d_1 and d_2 is the distance measured by the left and right LiDAR respectively and l is the fixed distance separating them along b_2. This setup is considerably simpler than using a depth camera and runs at a much higher rate but it gives less information about the perching surface. The pilot needs to look at the targeted surface before initiating the autonomous perching sequence to verify that it is flat and large enough to allow for the UAV to perch.

As illustrated in the lefthand side of Fig. 7, the UAV is first guided to a preliminary position at a fixed distance d_{pre} from the surface and it positions itself perpendicular to the surface.

When the the UAV is perpendicular to the surface (within 2 deg.), it begins to fly towards the surface at the preset ideal constant speed, v_{dock}. Once an impact has been detected by the force sensor, the UAV then holds its position for 0.5 s and waits for the pressure to drop. If the pressure sensor indicates a drop of pressure below the safe threshold of P_{land} = 880 hPa, the UAV considers the perching manoeuvre to be successful and it starts to decrease its thrust gradually. If pressure inside the suction cup does not drop low enough after the 0.5 s period, the UAV goes back to the position it was before the perching attempt and will retry the perching sequence.

The takeoff sequence follows the procedure shown in the right of Fig. 7. Starting from its current attitude, the UAV lowers its pitch to 0 deg. Once horizontal and stabilized, the pump is turned off and the UAV is commanded to hold its attitude. Finally, when the pressure sensor indicates that the pressure is over the safe threshold, the UAV detaches from the wall, moves back to the pre-perching location and waits for further instructions.

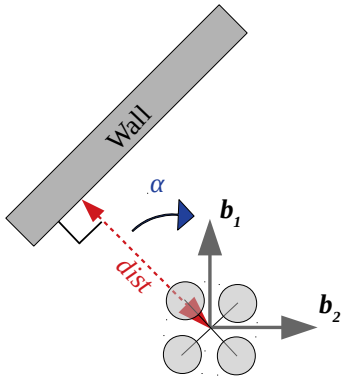

Fig. 8. Schematic of the pre-perching setup.

V. Experiments

Autonomous perching and takeoff on vertical surfaces has been achieved in simulation and in experimental tests as shown in Figs. 9 and 10. Fig. 9 shows video frames from an automated experimental and simulated perching sequence. Fig. 10 shows video frames from an automated experimental and simulated takeoff sequence.

A. Perching on a Flat Concrete Wall

Before launching the manoeuvre to perch on the concrete wall, the UAV is first positioned perpendicular to the wall at a distance of 1.5 meters as discussed in Section IV.

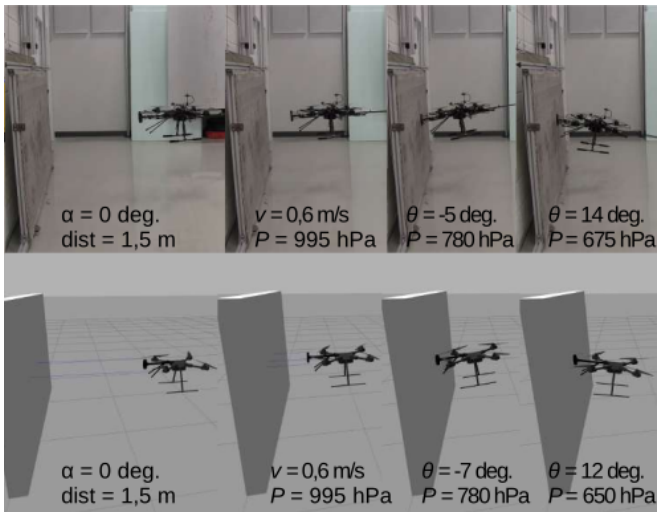

Fig. 9. Autonomous perching on a porous concrete wall: experimental (top), simulation (bottom).

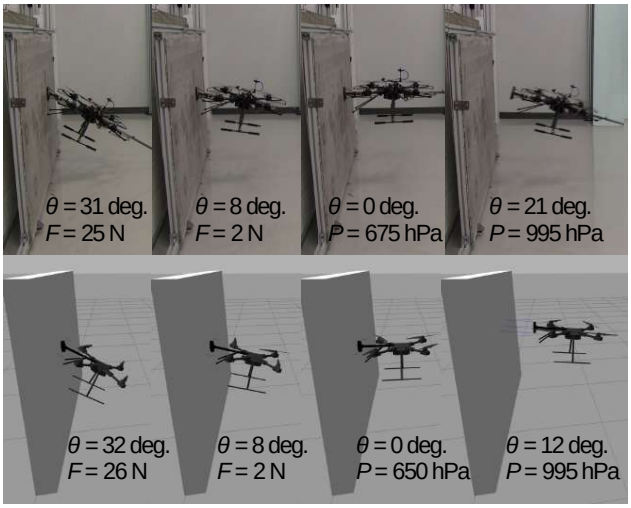

Fig. 10. Autonomous takeoff from a porous concrete wall: experimental (top), simulation (bottom).

Fig. 11 shows data from a complete perching procedure: the UAV accelerates to reach the desired impact speed (at 0.5 s for the simulation and at 2 s for the experiment). Then, a negative force spike is observed a few seconds later telling the controller that the vehicle has hit the wall. The final approach (between the downward pitch and the impact) is shorter in the experiment because the vehicle started the final perching approach closer to the wall. Once a successful attachment is achieved, defined by a drop of pressure below the safe threshold of P_{land} = 880 hPa, the UAV increases its pitch in order to land on the wall. Simultaneously, force applied on the suction cup increases as lift drops. The thrust slowly decreases until pitch stabilizes, indicating that the UAV is perched and the motors can be shut down.

Data from the autonomous takeoff and detachment procedure is similarly shown in Fig. 12. At the beginning of the sequence, the pressure is below the safe threshold. The UAV turns on its motors and increases its throttle. The

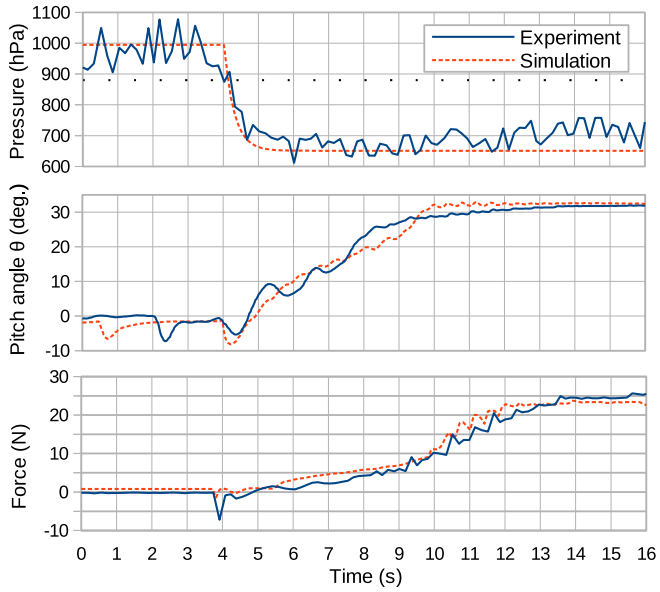

Fig. 11. Pressure, pitch angle, and force data from an autonomous perching from a concrete wall.

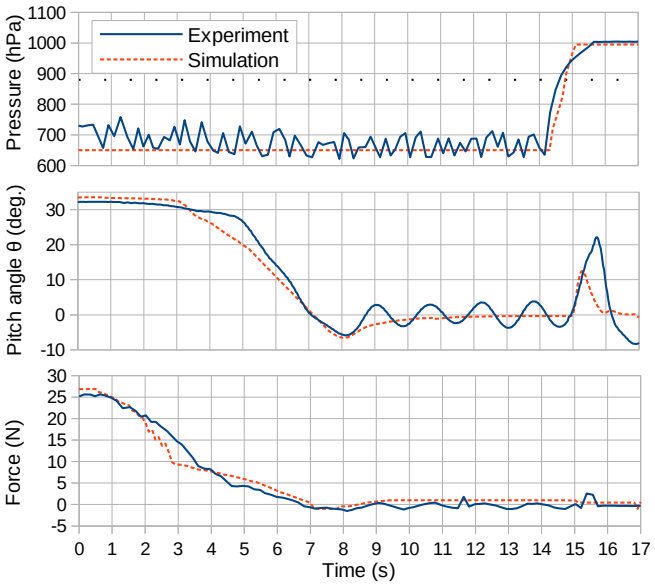

Fig. 12. Pressure, pitch angle and force data from an autonomous takeoff and detachment from a concrete wall.

pitch progressively decreases which reduces the force applied on the perching mechanism. When the UAV is horizontal, the vacuum pump is turned off and the pitch is kept at zero until the pressure is high enough for detachment. The airflow leaking through the concrete allows the pressure to build up fairly quickly, in about one second. Finally, the UAV detaches from the surface and moves back to the pre-perching location. It can be noticed in Fig. 12 that while waiting for the pressure to go back to atmospheric value, the pitch of the real vehicle oscillates while in simulation it remains stable.

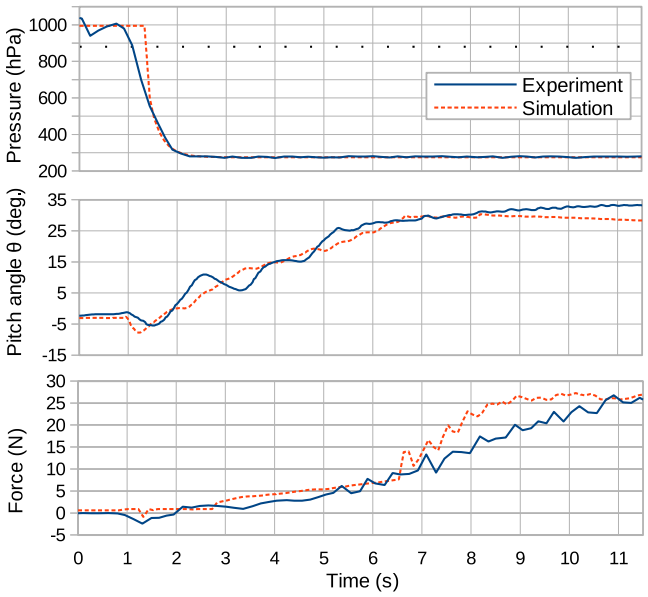

Fig. 13. Pressure, pitch angle and force data from an autonomous perching from a metallic surface.

B. Perching on a Flat Metallic Surface

Fig. 13 and 14 show the same manoeuvres as discussed in the previous section but on a metallic surface instead of a porous concrete wall. For the perching manoeuvre, the main difference observed in Fig. 13 compared with previous results is that since the metallic surface is smooth, the seal is better and the pressure in the suction cup drops as low as 275 hPa. Additionally, pressure fluctuations from the pump are no longer visible during experiments as the pump can turn off and the vacuum is maintained.

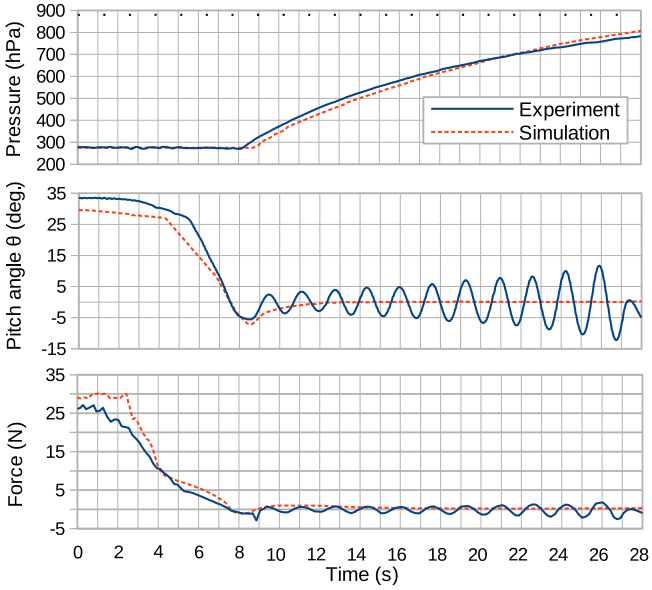

Fig. 14. Pressure, pitch angles and force data from an autonomous takeoff and detachment from a metallic surface.

However, as shown in Fig. 14, the detachment sequence goes quite differently compared with the concrete wall. Since the pressure level increases very slowly, the UAV has to remain stationary for much longer. Consequently, the pitch oscillations already observed in Fig. 12 last longer and their amplitudes grow larger, exceeding 5 deg. after 16 s. The detachment sequence is interrupted to avoid any incident. Similarly to the previous flight, the simulation does not predict these pitch oscillations and it is most likely because there are aerodynamic effects that are not well captured in the model. Tuning the controller for this scenario could alleviate the issue but it would be preferable to add a pneumatic solenoid valve to break the vacuum instantly. The detachment sequence would be quicker and much more predictable.

C. Failed Perching

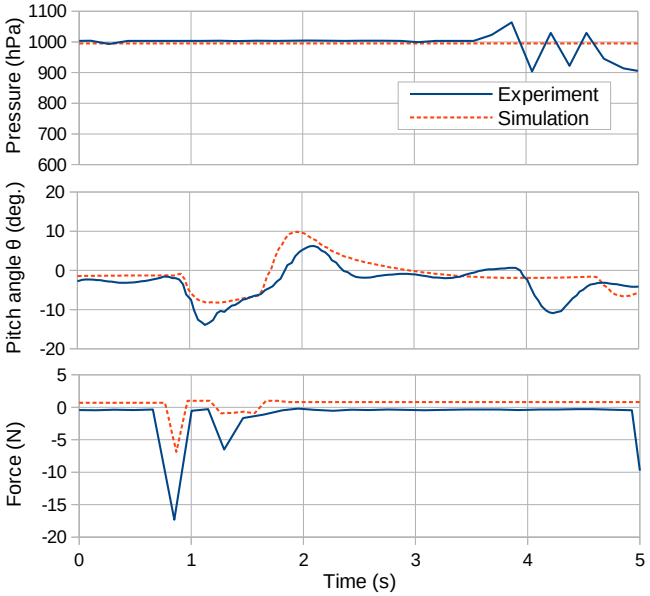

Fig. 15. Pitch angle and force data from a failed perching attempt.

Fig. 15 illustrates a failed perching attempt on a concrete surface. Similarly to Figs. 11 and 13, a peak of force immediately followed by a downward pitch indicates that the UAV has hit the surface. However, contrary to Fig. 11 and 13, the pressure in the suction cup does not drop as expected because the suction cup does not achieve a proper seal. After 0.5 s, the UAV detects the failed attempt, moves back to the pre-perching position and will try a new perching attempt.

VI. Conclusion

This work has presented an autonomous perching and take-off method for a multi-rotor UAV using a suction cup perching mechanism and LiDARs. The experimental results validated the method developed in simulation and show that the perching sequence was accurately modeled. The simulation model could be used to explore new perching mechanisms and develop vision-based perching methods. Future work should focus on improving the aerodynamic model to better simulate the interaction between the UAV and the landing surface.

REFERENCES

[1] V. Baiocchi, D. Dominici, and M. Mormile, "UAV application in post-seismic environment," *The International Archives of the Photogrammetry, Remote Sensing and Spatial Information Sciences*, vol. XL-1/W2, pp. 21–25, Aug. 2013. [Online]. Available: https://www.int-arch-photogramm-remote-sens-spatial-inf-sci.net/XL-1-W2/21/2013/

[2] J. H. Lee, S. Yoon, B. Kim, G.-H. Gwon, I.-H. Kim, and H.-J. Jung, "A new image-quality evaluating and enhancing methodology for bridge inspection using an unmanned aerial vehicle," *Smart Structures and Systems*, vol. 27, no. 2, pp. 209–226, 2021.

[3] P. Hamelin, F. Mirallès, G. Lambert, S. Lavoie, N. Pouliot, M. Montfrond, and S. Montambault, "Discrete-time control of LineDrone: An assisted tracking and landing UAV for live power line inspection and maintenance," in *2019 International Conference on Unmanned Aircraft Systems (ICUAS)*, Jun. 2019, pp. 292–298.

[4] A. Kulsinskas, P. Durdevic, and D. Ortiz-Arroyo, "Internal Wind Turbine Blade Inspections Using UAVs: Analysis and Design Issues," *Energies*, vol. 14, no. 2, p. 294, Jan. 2021. [Online]. Available: https://www.mdpi.com/1996-1073/14/2/294

[5] K. Hang, X. Lyu, H. Song, J. A. Stork, A. M. Dollar, D. Kragic, and F. Zhang, "Perching and resting—A paradigm for UAV maneuvering with modularized landing gears," *Science Robotics*, vol. 4, no. 28, p. eaau6637, Mar. 2019. [Online]. Available: https://robotics.sciencemag.org/lookup/doi/10.1126/scirobotics.aau6637

[6] J. D. Ang, L. Librado, C. J. Salaan, J. Maglasang, K. Sanchez, and M. Ang, "Drone with pneumatic-tethered suction-based perching mechanism for high payload application," in *2022 IEEE/RSJ International Conference on Intelligent Robots and Systems (IROS)*, 2022, pp. 12 154–12 161.

[7] S. Liu, W. Dong, Z. Ma, and X. Sheng, "Adaptive aerial grasping and perching with dual elasticity combined suction cup," *IEEE Robotics and Automation Letters*, vol. 5, no. 3, pp. 4766–4773, 2020.

[8] H. Tsukagoshi, M. Watanabe, T. Hamada, D. Ashlih, and R. Iizuka, "Aerial manipulator with perching and door-opening capability," in *2015 IEEE International Conference on Robotics and Automation (ICRA)*, May 2015, pp. 4663–4668.

[9] H. Wopereis, D. Ellery, T. Post, S. Stramigioli, and M. Fumagalli, "Autonomous and sustained perching of multirotor platforms on smooth surfaces," in *2017 25th Mediterranean Conference on Control and Automation (MED)*, Jul. 2017, pp. 1385–1391.

[10] J. Meyer, A. Sendobry, S. Kohlbrecher, U. Klingauf, and O. von Stryk, "Comprehensive simulation of quadrotor uavs using ros and gazebo," in *Simulation, Modeling, and Programming for Autonomous Robots*, I. Noda, N. Ando, D. Brugali, and J. J. Kuffner, Eds. Berlin, Heidelberg: Springer Berlin Heidelberg, 2012, pp. 400–411.

[11] S. Shah, D. Dey, C. Lovett, and A. Kapoor, "Airsim: High-fidelity visual and physical simulation for autonomous vehicles," in *Field and Service Robotics*, M. Hutter and R. Siegwart, Eds. Cham: Springer International Publishing, 2018, pp. 621–635.

[12] M. Schmittle, A. Lukina, L. Vacek, J. Das, C. P. Buskirk, S. Rees, J. Sztipanovits, R. Grosu, and V. Kumar, "OpenUAV: A UAV Testbed for the CPS and Robotics Community," in *2018 ACM/IEEE 9th International Conference on Cyber-Physical Systems (ICCPS)*. Porto: IEEE, Apr. 2018, pp. 130–139.

[13] K. Xiao, S. Tan, G. Wang, X. An, X. Wang, and X. Wang, "XTDrone: A Customizable Multi-rotor UAVs Simulation Platform," in *2020 4th International Conference on Robotics and Automation Sciences (ICRAS)*. Wuhan, China: IEEE, Jun. 2020, pp. 55–61.

[14] M. Vernacchia, "Gazebo Motor & Propeller Model Notes," p. 8.